Protein Structure Parameterization via Möbius Distributions on the Torus

Mohammad Arashi [1,4], Najmeh Nakhaei Rad [*2,3,4], Andriëtte Bekker[4], Wolf Dieter Schubert[5]

[1] Department of Statistics, Faculty of Mathematical Sciences, Ferdowsi University of Mashhad, Iran.

[2]Department of Mathematics and Statistics, Mashhad Branch, Islamic Azad University, Mashhad, Iran.

[3]DSI-NRF Centre of Excellence in Mathematical and Statistical Sciences (CoE-MaSS), South Africa.

[4]Department of Statistics, University of Pretoria, Pretoria 0002, South Africa.

[5]Department of Biochemistry, University of Pretoria, Pretoria 0002, South Africa.

Abstract

Proteins constitute a large group of macromolecules with a multitude of functions for all living organisms. Proteins achieve this by adopting distinct three-dimensional structures encoded by the sequence of their constituent amino acids in one or more polypeptides. In this paper, the statistical modelling of the protein backbone torsion angles is considered. Two new distributions are proposed for toroidal data by applying the Möbius transformation to the bivariate von Mises distribution. Marginal and conditional distributions in addition to sine-skewed versions of the proposed models are also developed. Three big data sets consisting of bivariate information about protein domains are analysed to illustrate the strength of the flexible proposed models. Finally, a simulation study is done to evaluate the obtained maximum likelihood estimates and also to find the best method of generating samples from the proposed models to use as the proposal distributions in the Markov Chain Monte Carlo sampling method for predicting the 3D structure of proteins.

Keywords: Biostatistics; Cosine Model; Möbius transformation; Sine model; Toroidal data; Torus.

1 Introduction

Proteins constitute a diverse set of biological macromolecules. Due to their central role in most biological processes, proteins are often referred to as the workhorses of cells. Chemically, proteins are biopolymers consisting of linear sequences of amino acid residues linked by covalent peptide bonds such that each polypeptide is a single large molecule. The twenty natural amino acids (except proline) all have an amino group ($–NH_2$), a carboxylic acid group ($–COOH$), an amino-acid specific side-chain and a hydrogen atom attached to a central carbon atom (C_α). The peptide bond links the carboxylate group of one amino acid to the amino group of the next. Protein structure is often thought of in four levels of organization: The primary structure is the sequence of amino acids. The secondary structure accounts for the local folding of the polypeptide backbone into helices, strands or loops. The tertiary structure describes the three-dimensional fold of the protein. Finally the quaternary structure describes the involvement of one or more chains in creating the functional protein. The amino nitrogen, the C_α and the carbonyl carbon of all residues constitute the protein backbone.

*Corresponding author: najme.rad@gmail.com

The 3D coordinates of proteins, as provided by electron microscopy or X-ray crystallography, directly reveal the conformation of the backbone atoms, though knowledge of standard chemical bond angles and lengths is used during the refinement process. Generally, the backbone conformation is analysed using the backbone torsion or dihedral angles denoted ϕ, ψ and ω as introduced by Ramachandran (Ramachandran and Sasisekharan, 1968) (Fig. 1(A)), where ω is usually close to 180° or occasionally 0°. Alternatively, virtual bond and torsion angles θ and τ may be used to describe a protein backbone representation based on C_α positions only (Fig. 1(B)). A major concern and challenge in molecular biology and computational

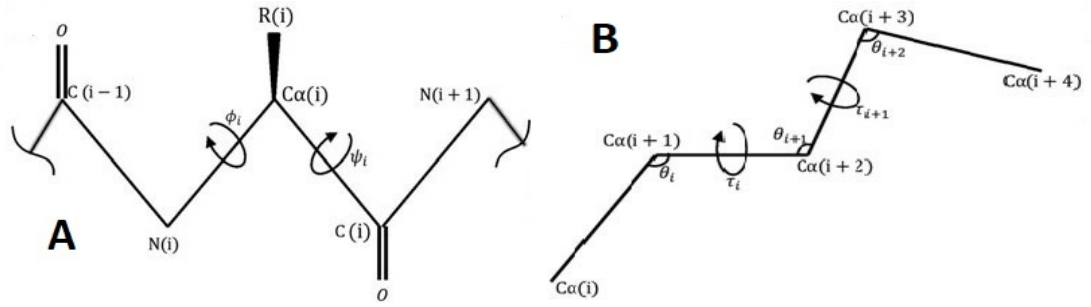

Figure 1: Two representations of protein backbone structures based on torsion or pseudo-torsion angles.

biochemistry involves predicting the 3D structure of proteins. While the primary structure of a protein is provided by the encoding gene, the secondary structure may be predicted computationally with high reliability using artificial neural networks (Holley and Karplus, 1989) based on the propensity of amino acids to form different secondary structures. Predicting the 3D structure of a protein, especially if larger than 100 amino acid residues or if a homologue with significant sequence identity is not available, however, remains challenging. This challenge is addressed by *de novo* structure prediction that requires parametrized physical force fields. The probability of observing a particular conformation $\boldsymbol{x}$ of the molecule, $p(\boldsymbol{x}|\beta)$ is considered and expressed as the Boltzmann distribution:

$$p(\boldsymbol{x}|\beta) = \frac{\exp(\beta U(\boldsymbol{x}))}{Z_\beta},$$

where Z_β is the normalization constant, $U(\boldsymbol{x})$ is the potential energy of the molecule, $\beta = (k_b T)^{-1}$ is the thermodynamic beta, k_b is the Boltzmann constant and constant T is the temperature. The 3D structure of the molecule can be derived from $p(\boldsymbol{x}|\beta)$ by finding the mode of the distribution. Molecular dynamics (MD) is a simulation-based method used to probe this. However, many million to trillion steps are needed to simulate a single folding event. In comparison with MD, Monte Carlo (MC) based methods are more time efficient. In Markov Chain Monte Carlo (MCMC), a Markov chain is constructed using the Metropolis Hastings (MH) algorithm (Metropolis et al., 1953 and Hastings, 1970) that has $p(\boldsymbol{x}|\beta)$ as stationary distribution. A symmetric proposal distribution is utilized in the MH algorithm. Choosing a good proposal distribution is one of the challenges in MCMC-based simulation. Gaussian perturbations are the most straightforward proposal distributions that can be used (Irbäck and Mohanty, 2006). When proposal distribution is closer to the stationary distribution, the results are more accurate; due to this, protein structural information is incorporated into most proposal distributions. Using the information of angles or stretches of angles that are observed in real proteins is a simple way to define a suitable proposal distribution. Fragment libraries for backbone angles and rotamer libraries for side chain angles can be used as the standard choices for proposal distributions (Jones, 1997, Jones and Thirup, 1986 and Simons et al., 1997). Various tractable statistical

distributions for modelling the dihedral angles in proteins are briefly reviewed. These models will not generate folded proteins because they work under some simplifying assumptions, both in terms of functional form and dependency structure. In fact, these models can be used as proposal distributions for MCMC sampling of proteins. The models can also be utilized as a prior for protein structure determination from data. The ultimate goal of our contribution is to propose more flexible models for the proposal distribution. For instance, Olsson et al. (2011) demonstrated that both the accuracy and speed in inferential structure determination from nuclear magnetic resonance (NMR) data were improved by using these statistical models (see Ley and Verdebout, 2017, 2018).

The first probability distribution on the dihedral angles was proposed by Mardia (1975) namely the bivariate von Mises distribution:

$$\begin{aligned} f(\theta_1,\theta_2) &= C\exp(\kappa_1\cos(\theta_1-\iota_1)+\kappa_2\cos(\theta_2-\iota_2) \\ &+ (\cos(\theta_1-\iota_1),\sin(\theta_1-\iota_1))\,A\,(\cos(\theta_2-\iota_2),\sin(\theta_2-\iota_2))^T), \end{aligned}$$

where C is the normalizing constant, $\iota_1,\iota_2\in[-\pi,\pi)$ are location parameters, $\kappa_1,\kappa_2\geq 0$ are concentration parameters and matrix $A_{2\times 2}$ is the circular-circular dependence parameter. Because of the large number of parameters of the bivariate von Mises distribution, some special cases were considered. Rivset (1988) introduced a subclass of distributions as follows:

$$\begin{aligned} f(\theta_1,\theta_2) &\propto \exp(\kappa_1\cos(\theta_1-\iota_1)+\kappa_2\cos(\theta_2-\iota_2)+\alpha\cos(\theta_1-\iota_1)\cos(\theta_2-\iota_2) \\ &+ \beta\sin(\theta_1-\iota_1)\sin(\theta_2-\iota_2)), \end{aligned} \tag{1}$$

where $\alpha,\beta\in\mathbb{R}$. Since the probability density function (pdf) in (1) was still overparameterized, Singh et al. (2002) proposed a special case by substituting $\alpha=0$ and $\beta=\kappa_3$, which is called the *Sine model* with pdf:

$$f(\theta_1,\theta_2)=C\exp(\kappa_1\cos(\theta_1-\iota_1)+\kappa_2\cos(\theta_2-\iota_2)+\kappa_3\sin(\theta_1-\iota_1)\sin(\theta_2-\iota_2)), \tag{2}$$

where

$$C^{-1}=4\pi^2\sum_{i=0}^{\infty}\binom{2i}{i}\left(\frac{\kappa_3^2}{4\kappa_1\kappa_2}\right)^i I_i(\kappa_1)I_i(\kappa_2), \tag{3}$$

and $I_\alpha(z)$ is the modified Bessel function of the first kind of order α. Another submodel of (1) was introduced by Mardia et al. (2007) in a similar manner by setting $\alpha=\beta=-\kappa_3$, which is known as the *Cosine model* with the following pdf:

$$f(\theta_1,\theta_2)=C\exp(\kappa_1\cos(\theta_1-\iota_1)+\kappa_2\cos(\theta_2-\iota_2)-\kappa_3\cos(\theta_1-\iota_1-\theta_2+\iota_2)), \tag{4}$$

where

$$C^{-1}=4\pi^2\left\{I_0(\kappa_1)I_0(\kappa_2)I_0(\kappa_3)+2\sum_{i=1}^{\infty}I_i(\kappa_1)I_i(\kappa_2)I_i(\kappa_3)\right\}. \tag{5}$$

The main motivation for defining toroidal models in recent years has been the demand from other sciences, especially bioinformatics, for modelling dihedral angels to analyse protein structures (Singh et al., 2002, Mardia et al., 2007, Di Marzio et al., 2011, Ameijeiras-Alonso and Ley, 2019) and using these as proposal distributions for MCMC sampling of proteins. But the toroidal data can also be observed in other areas; for example, in meteorology (the wind directions at two different times of the day) and medicine (the peak systolic blood pressure during two separate time periods). Some applications of toroidal models can be found in Kato et al. (2008), Shieh and Johnson (2005), Shieh et al. (2011), Liu et al. (2006) and Downs and Mardia (2002).

A common method of creating flexible new distributions is to apply suitable transformations, which can be defined on the real line or on the circle. Minh and Farnum (2003) employed a bilinear transformation, which mapped the unit circle into the real line to induce probability distributions on the real line. Jones (2004) applied the Möbius transformation to introduce a new family of distributions on the disc. Kato and Jones (2010) used the Möbius transformation to transform circles to circles and introduced a new distribution on the circle by transforming the von Mises distribution. Wang and Shimizu (2012) applied the Möbius transformation to the cardioid random variables. Kato and Pewsey (2015) employed the Möbius transformation to define a new distribution on the torus by transforming the bivariate circular distribution of Kato (2009). Kato and McCullagh (2018) introduced the Cauchy distribution on the sphere by using the Möbius transformation. In this paper, two new distributions are introduced on the torus by applying the Möbius transformation. The Möbius transformation transforms θ into $\tilde{\theta}$ through the mapping:

$$\theta = \mho(\tilde{\theta}, \mu, \nu, r) = \mu + \nu + 2arctan\left\{\frac{1-r}{1+r}tan\left(\frac{\tilde{\theta}-\nu}{2}\right)\right\}, \tag{6}$$

where $-\pi \leq \mu, \nu \leq \pi$ and $r \in [0, 1)$. If $r = 0$, the transformation would be the identity mapping and when $r \to 1$ the $\mho(\tilde{\theta}, \mu, \nu, r)$ tends to ν. More details about the Möbius transformation can be found in Downs and Mardia (2002) and McCullagh (1996). The inverse of (6) can be obtained as:

$$\tilde{\theta} = \nu + 2arctan\left\{\frac{1+r}{1-r}tan\left(\frac{\theta-\mu-\nu}{2}\right)\right\}.$$

The paper is organized as follows. In Section 2, two new distributions are defined by transforming the Sine and Cosine models in (2) and (4), and some of their properties are studied. Section 3 is dedicated to introducing the sine-skewed version of the newly proposed transformed Sine and Cosine models. In Section 4, the maximum likelihood estimations (MLE) of parameters are derived for the proposed models. Three real data sets, including the information of angles in the protein structure, are analysed in Section 5 to demonstrate the performance of the proposed models. In Section 6, a simulation study is carried out to find the best method of generating samples from the new transformed Sine and Cosine distributions to use as proposal distributions in MCMC sampling for predicting the 3D structure of proteins and also for evaluating the obtained maximum likelihood estimates in Section 4.

2 Two New Models On The Torus

In this section, two new models are proposed for toroidal data by transforming the Sine and Cosine models in (2) and (4) via the Möbius transformation.

Definition 2.1. *Let* $(\tilde{\Theta}_1, \tilde{\Theta}_2)$ *have pdf* (4) *with* $\iota_1 = \iota_2 = 0$. *Suppose*

$$(\Theta_1, \Theta_2) = \left(\mho(\tilde{\Theta}_1, \mu_1, \nu_1, r_1), \mho(\tilde{\Theta}_2, \mu_2, \nu_2, r_2)\right),$$

where $\mho(.)$ *is defined in* (6), $\mu_1, \mu_2, \nu_1, \nu_2 \in (-\pi, \pi]$, $r_1, r_2 \in [0, 1)$ *and without loss of generality* $\nu_1 = \nu_2 = 0$. *Then* (Θ_1, Θ_2) *have pdf*

$$\begin{aligned} f(\theta_1, \theta_2) &= \frac{C(1-r_1^2)(1-r_2^2)}{(1+r_1^2-2r_1\cos(\theta_1-\mu_1))(1+r_2^2-2r_2\cos(\theta_2-\mu_2))} \\ &\times \exp\left\{\frac{1}{(1+r_1^2-2r_1\cos(\theta_1-\mu_1))(1+r_2^2-2r_2\cos(\theta_2-\mu_2))}(C_0 + C_1\cos(\theta_1-\mu_1)\right. \\ &\left. + C_2\cos(\theta_2-\mu_2) + C_3\cos(\theta_1-\mu_1)\cos(\theta_2-\mu_2) + C_4\sin(\theta_1-\mu_1)\sin(\theta_2-\mu_2))\right\}, \end{aligned} \tag{7}$$

where $\kappa_1, \kappa_2 \geq 0$, $\kappa_3 \in \mathbb{R}$, C *is defined in* (5) *and*

$$\begin{aligned}
C_0 &= -2\kappa_1 r_1(1+r_2^2) - 2\kappa_2 r_2(1+r_1^2) - 4\kappa_3 r_1 r_2, \\
C_1 &= \kappa_1(1+r_1^2)(1+r_2^2) + 2\kappa_3 r_2(1+r_1^2) + 4\kappa_2 r_1 r_2, \\
C_2 &= \kappa_2(1+r_1^2)(1+r_2^2) + 2\kappa_3 r_1(1+r_2^2) + 4\kappa_1 r_1 r_2, \\
C_3 &= -2\kappa_1 r_2(1+r_1^2) - 2\kappa_2 r_1(1+r_2^2) - \kappa_3(1+r_1^2)(1+r_2^2), \\
C_4 &= -\kappa_3(1-r_1^2)(1-r_2^2).
\end{aligned} \tag{8}$$

In (7) when $r_1 = r_2 = 0$, the *Cosine model* in (4) is obtained. $\kappa_1, \kappa_2, \kappa_3 = 0$ yield the bivariate wrapped Cauchy distribution when $\theta_1 \perp \theta_2$. The pdf and contour plots of (7) are shown in Fig. 2 for $\mu_1 = \mu_2 = 0$ and different values of $\kappa_1, \kappa_2, \kappa_3, r_1$ and r_2. As can be seen, the *transformed Cosine* model in (7) can be both unimodal and bimodal.

Theorem 2.2. *For the transformed Cosine model in* (7)*, when* $r_1, r_2 \to 0$*, then* (Θ_1, Θ_2) *has approximately a bivariate normal distribution if and only if* $\kappa_3 \leq \frac{\kappa_1\kappa_2}{\kappa_1+\kappa_2}$.

Proof. When $r_1, r_2 \to 0$, the pdf in (7) tends to the Cosine distribution, which for large values of κ_1 and κ_2 is concentrated near 0. Suppose $\mu_1 = \mu_2 = 0$ (without loss of generality), according to Theorem 1 in Mardia et al. (2007) and using Taylor expansions, $(\Theta_1, \Theta_2) \sim N_2(0, \Sigma)$, where $\Sigma^{-1} = \begin{pmatrix} \kappa_1 - \kappa_3 & \kappa_3 \\ \kappa_3 & \kappa_2 - \kappa_3 \end{pmatrix}$. It is necessary to have $\kappa_3 \leq \frac{\kappa_1\kappa_2}{\kappa_1+\kappa_2}$. □

In the following, the marginal pdf and conditional pdf of the transformed Cosine model and their properties are discussed. The marginal pdf of θ_1 for the transformed Cosine model in (7) is as follows:

$$f_{\Theta_1}(\theta_1) = \frac{2\pi C(1-r_1^2)}{1+r_1^2-2r_1\cos(\theta_1-\mu_1)} I_0(h(\theta_1)) \exp\left\{\frac{\kappa_1(1+r_1^2)\cos(\theta_1-\mu_1) - 2\kappa_1 r_1}{1+r_1^2-2r_1\cos(\theta_1-\mu_1)}\right\}, \tag{9}$$

where

$$h(\theta_1) = \left\{\kappa_2^2 + \kappa_3^2 - \frac{2\kappa_2\kappa_3\left((1+r_1^2)\cos(\theta_1-\mu_1) - 2r_1\right)}{1+r_1^2-2r_1\cos(\theta_1-\mu_1)}\right\}^{1/2}, \tag{10}$$

and C is defined in (5). The marginal pdf of Θ_1 in (9) is symmetric about μ_1, for small values of κ_3 is approximately the transformed von Mises distribution (Kato and Jones, 2010) and for $r_1 = 0$, is the marginal pdf of the Cosine model (Mardia et al., 2007). It is clear that for $r_1 = 0$ and small values of κ_3, it is approximately the von Mises distribution. If $\kappa_1 = \kappa_2 = \kappa_3 = 0$ in (9), the transformed uniform distribution is obtained. For $\kappa_1 = \kappa_2 = \kappa_3 = r_1 = 0$, the distribution is uniform. When $\kappa_1 = \kappa_2 = 0$ in (9), the distribution is the transformed von Mises (Kato and Jones, 2010), and when $\kappa_1 = \kappa_2 = r_1 = 0$, the von Mises distribution is obtained. The plots of the marginal pdf of Θ_1 are shown in Fig. 3 for $\mu_1 = 0$ and different values of $\kappa_1, \kappa_2, \kappa_3$ and r_1. As can be seen, it can be both unimodal and bimodal. In the following theorem, the bimodality of the marginal density function Θ_1 is discussed.

Theorem 2.3. *The marginal distribution of* Θ_1 *in* (9) *is symmetric around* $\theta_1 = \mu_1$ *and unimodal (with mode at* μ_1*) if and only if* $\frac{A(|\kappa_2-\kappa_3|)}{|\kappa_2-\kappa_3|} \leq \left(\frac{2r_1(1-r_1)^2}{(1-r_1^2)^2} + \kappa_1\right)/\kappa_2\kappa_3$ *where* $A(\kappa) = I_1(\kappa)/I_0(\kappa)$*. Also, the marginal distribution of* Θ_1 *in* (9) *is bimodal (with the modes at* $\mu_1 - \theta_1^*$ *and* $\mu_1 + \theta_1^*$*) if and only if* $\frac{A(|\kappa_2-\kappa_3|)}{|\kappa_2-\kappa_3|} > \left(\frac{2r_1(1-r_1)^2}{(1-r_1^2)^2} + \kappa_1\right)/\kappa_2\kappa_3$ *and* θ_1^* *is the result of* $\kappa_2\kappa_3(1-r_1^2)^2 A(h(\theta_1^*))/h(\theta_1^*) - 2r_1(1+r_1^2-2r_1\cos(\theta_1^*-\mu_1)) - \kappa_1(1-r_1^2)^2 = 0$ *where* $h(\theta)$ *is defined in* (10).

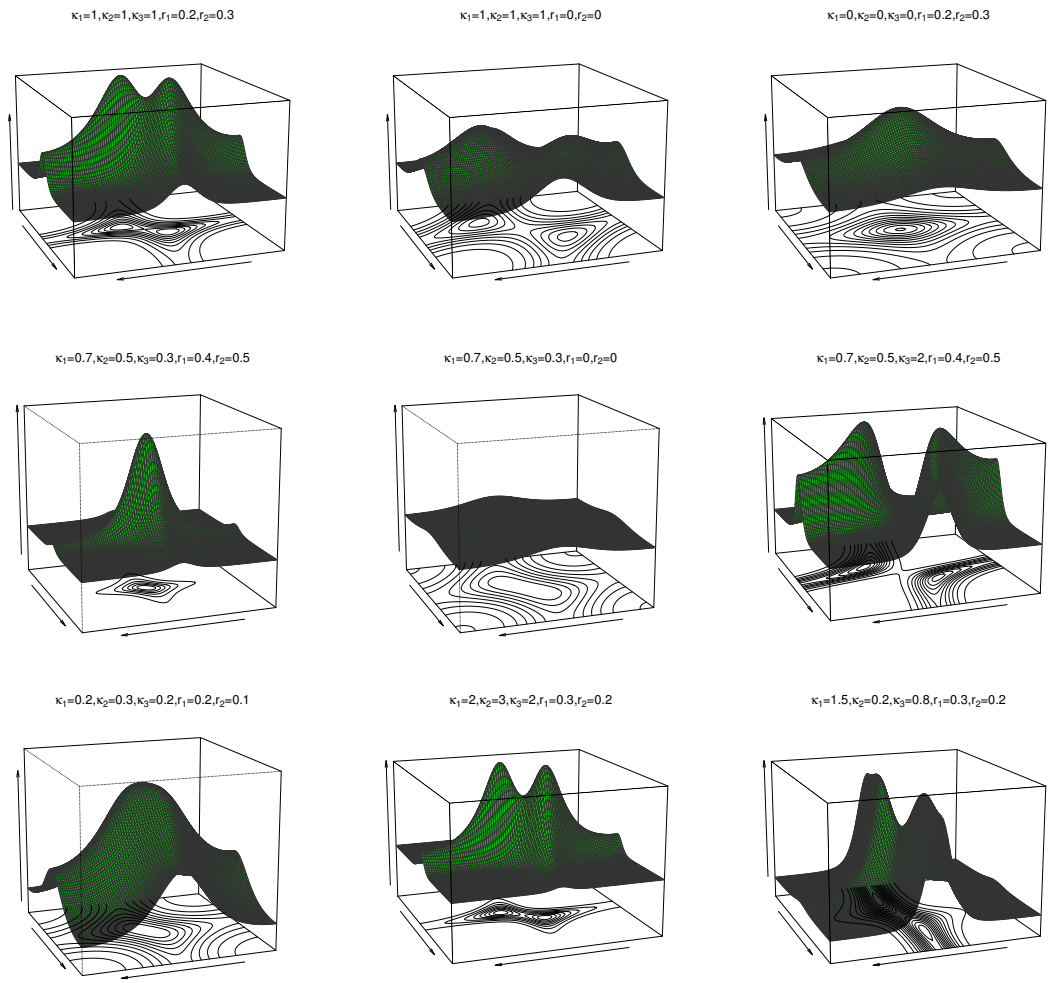

Figure 2: The pdf and contour plots of the transformed Cosine model in (7) for $\mu_1 = \mu_2 = 0$ and different values of $\kappa_1, \kappa_2, \kappa_3, r_1$ and r_2.

Proof. Without loss of generality, it is considered that $\mu_1 = 0$. According to (9), it is concluded that

$$\begin{aligned}\frac{f'_{\Theta_1}(\theta_1)}{f_{\Theta_1}(\theta_1)} &= \left\{ \frac{-2r_1}{(1+r_1^2-2r_1\cos\theta_1)} + \frac{\kappa_2\kappa_3(1-r_1^2)^2 A(h(\theta_1))}{h(\theta_1)(1+r_1^2-2r_1\cos\theta_1)^2} \right. \\ &\quad \left. - \frac{\kappa_1(1-r_1^2)^2}{(1+r_1^2-2r_1\cos\theta_1)^2} \right\} \sin\theta_1 \\ &= g(\theta_1)\sin\theta_1. \end{aligned} \tag{11}$$

In (11), if $\kappa_3 < 0$ then $g(\theta_1) < 0$. So, for $\theta_1 \in [0, \pi)$, $f'_{\Theta_1}(\theta_1) < 0$ and for $\theta_1 \in [-\pi, 0)$, $f'_{\Theta_1}(\theta_1) \geq 0$. Thus, $f_{\Theta_1}(\theta_1)$ is increasing in $[-\pi, 0)$ and decreasing from 0 to π. In addition, $f_{\Theta_1}(\theta_1) = f_{\Theta_1}(-\theta_1)$, which means that $f_{\Theta_1}(\theta_1)$ is symmetric around 0; so, for $\kappa_3 < 0$, $f_{\Theta_1}(\theta_1)$ is unimodal. If $\kappa_3 > 0$, $h(\theta_1)$ is decreasing from $-\pi$ to 0 and increasing from 0 to π and $h(0) =\mid \kappa_2 - \kappa_3 \mid$ and $h(-\pi) = \kappa_2 + \kappa_3$. From Lemma

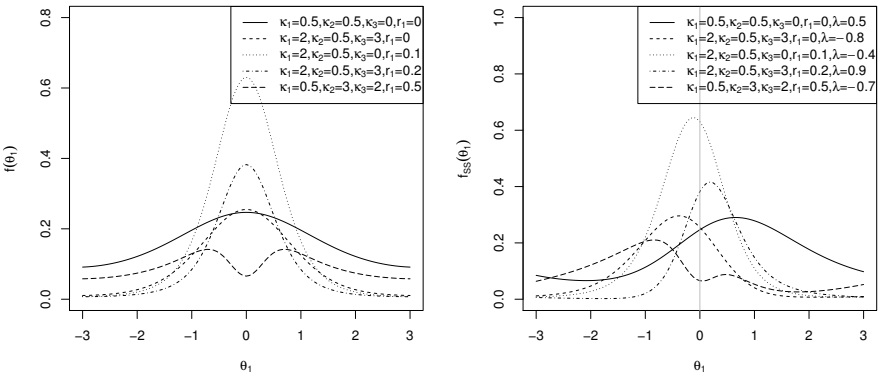

Figure 3: The plots of the marginal pdf of Θ_1 in (9) (left) and the skewed marginal pdf of Θ_1 in (12) (right) for $\mu_1 = 0$ and different values of parameters.

1 in Singh et al. (2002), $A(t)/t$ is a decreasing function of t; so, $A(h(\theta_1))/h(\theta_1)$ is increasing in $[-\pi, 0)$ and decreasing from 0 to π. It is concluded that $g(\theta_1)$ is decreasing in $[0, \pi)$ and increasing in $[-\pi, 0)$; so, if $-2r_1 + \kappa_2\kappa_3 \frac{A(|\kappa_2-\kappa_3|)}{|\kappa_2-\kappa_3|} \frac{(1-r_1^2)^2}{(1-r_1)^2} - \kappa_1 \frac{(1-r_1^2)^2}{(1-r_1)^2} < 0$, then $f'_{\Theta_1}(\theta_1) \geq 0$ for $\theta_1 \in [-\pi, 0)$ and $f'_{\Theta_1}(\theta_1) < 0$ for $\theta_1 \in [0, \pi)$; which means that $f_{\Theta_1}(\theta_1)$ is unimodal. If $-2r_1 + \kappa_2\kappa_3 \frac{A(|\kappa_2-\kappa_3|)}{|\kappa_2-\kappa_3|} \frac{(1-r_1^2)^2}{(1-r_1)^2} - \kappa_1 \frac{(1-r_1^2)^2}{(1-r_1)^2} > 0$ and $-2r_1 + \kappa_2\kappa_3 \frac{A(\kappa_2+\kappa_3)}{\kappa_2+\kappa_3} \frac{(1-r_1^2)^2}{(1+r_1)^2} - \kappa_1 \frac{(1-r_1^2)^2}{(1+r_1)^2} \leq 0$, then $f_{\Theta_1}(\theta_1)$ is first increasing and then decreasing in $[-\pi, 0)$, which means that $f_{\Theta_1}(\theta_1)$ is bimodal. □

Abe and Pewsey (2011) introduced the Sine-skewed distributions on the circle, which can be used here to introduce the skewed version of the marginal distribution of Θ_1 in (9) as:

$$f_{SS}(\theta_1) = \frac{2\pi C(1-r_1^2)}{1+r_1^2-2r_1\cos(\theta_1-\mu_1)} I_0(h(\theta_1)) \exp\left\{\frac{\kappa_1(1+r_1^2)\cos(\theta_1-\mu_1) - 2\kappa_1 r_1}{1+r_1^2-2r_1\cos(\theta_1-\mu_1)}\right\} \times (1+\lambda\sin(\theta_1-\mu_1)), \tag{12}$$

where C is defined in (5), $h(\theta_1)$ is defined in (10) and $-1 \leq \lambda \leq 1$. $\lambda > 0$ leads to left-skewed distributions and $\lambda < 0$ provides right-skewed distributions. The plots of the skewed pdf in (12) are shown in Fig. 3 for $\mu_1 = 0$ and different values of $\kappa_1, \kappa_2, \kappa_3, r_1$ and λ.

The conditional pdf, $f(\theta_2 \mid \Theta_1 = \theta_1)$, is the transformed von Mises distribution (Kato and Jones, 2010) given by:

$$f(\theta_2 \mid \Theta_1 = \theta_1) = \frac{1-r_2^2}{2\pi I_0(h(\theta_1))} \frac{1}{1+r_2^2-2r_2\cos(\theta_2-\mu_2)} \times \exp\left\{\frac{h(\theta_1)\cos\tau((1+r_2^2)\cos(\theta_2-\mu_2)-2r_2) + h(\theta_1)\sin\tau(1-r_2^2)\sin(\theta_2-\mu_2)}{1+r_2^2-2r_2\cos(\theta_2-\mu_2)}\right\}, \tag{13}$$

where $tan\tau = \frac{-\kappa_3(1-r_1^2)\sin(\theta_1-\mu_1)}{\kappa_2(1+r_1^2-2r_1\cos(\theta_1-\mu_1))-\kappa_3((1+r_1^2)\cos(\theta_1-\mu_1)-2r_1)}$. For $r_1 = 0$, (13) is the von Mises distribution with parameter τ and $h(\theta_1)$ in (10).

Definition 2.4. *Let* $(\tilde{\Theta}_1, \tilde{\Theta}_2)$ *have bivariate pdf in* (2) *with* $\iota_1 = \iota_2 = 0$. *Suppose*

$$(\Theta_1, \Theta_2) = \left(\mho(\tilde{\Theta}_1, \mu_1, \nu_1, r_1), \mho(\tilde{\Theta}_2, \mu_2, \nu_2, r_2)\right),$$

where $\mho(.)$ *is defined in* (6), $\mu_1, \mu_2, \nu_1, \nu_2 \in (-\pi, \pi]$, $r_1, r_2 \in [0, 1)$ *and without loss of generality* $\nu_1 = \nu_2 = 0$. *Then* (Θ_1, Θ_2) *have pdf*

$$\begin{aligned} f(\theta_1, \theta_2) &= \frac{C(1-r_1^2)(1-r_2^2)}{(1+r_1^2-2r_1\cos(\theta_1-\mu_1))(1+r_2^2-2r_2\cos(\theta_2-\mu_2))} \\ &\times \exp\left\{\frac{1}{(1+r_1^2-2r_1\cos(\theta_1-\mu_1))(1+r_2^2-2r_2\cos(\theta_2-\mu_2))}(C_0 + C_1\cos(\theta_1-\mu_1)\right. \\ &\left. + C_2\cos(\theta_2-\mu_2) + C_3\cos(\theta_1-\mu_1)\cos(\theta_2-\mu_2) + C_4\sin(\theta_1-\mu_1)\sin(\theta_2-\mu_2))\right\}, \end{aligned} \tag{14}$$

where $\kappa_1, \kappa_2 \geq 0$, $\kappa_3 \in \mathbb{R}$, C *is defined in* (3) *and*

$$\begin{aligned} C_0 &= -2\kappa_1 r_1(1+r_2^2) - 2\kappa_2 r_2(1+r_1^2), \\ C_1 &= \kappa_1(1+r_1^2)(1+r_2^2) + 4\kappa_2 r_1 r_2, \\ C_2 &= \kappa_2(1+r_1^2)(1+r_2^2) + 4\kappa_1 r_1 r_2, \\ C_3 &= -2\kappa_1 r_2(1+r_1^2) - 2\kappa_2 r_1(1+r_2^2), \\ C_4 &= \kappa_3(1-r_1^2)(1-r_2^2). \end{aligned} \tag{15}$$

When $r_1 = r_2 = 0$ in (14), then the *Sine model* in (2) is obtained. The pdf and the contour plots of (14) are shown in 4 for $\mu_1 = \mu_2 = 0$ and different values of $\kappa_1, \kappa_2, \kappa_3, r_1$ and r_2. As can be seen, the *transformed Sine* pdf in (14) can be both unimodal and bimodal.

Theorem 2.5. *For the transformed Sine model in* (14), *when* $r_1, r_2 \to 0$, *then* (Θ_1, Θ_2) *have approximately a bivariate normal distribution if and only if* $\kappa_3^2 < \kappa_1\kappa_2$.

Proof. Similar to Theorem 2.2, by using the results in Singh et al. (2002), the theorem is proved. □

The marginal pdf of Θ_1 for the transformed Sine model in (14) is as follows:

$$f_{\Theta_1}(\theta_1) = \frac{2\pi C(1-r_1^2)}{1+r_1^2-2r_1\cos(\theta_1-\mu_1)} I_0(h(\theta_1)) \exp\left\{\frac{\kappa_1(1+r_1^2)\cos(\theta_1-\mu_1) - 2\kappa_1 r_1}{1+r_1^2-2r_1\cos(\theta_1-\mu_1)}\right\}, \tag{16}$$

where

$$h(\theta_1) = \left\{\kappa_2^2 + \left(\frac{\kappa_3(1-r_1^2)}{1+r_1^2-2r_1\cos(\theta_1-\mu_1)}\right)^2 \sin^2(\theta_1-\mu_1)\right\}^{1/2}, \tag{17}$$

and C is defined (3). The marginal pdf of Θ_1 is symmetric about μ_1. If $\kappa_3 = 0$, the distribution is the transformed von Mises distribution (Kato and Jones, 2010). If $r_1 = 0$ in (16), the marginal distribution of the Sine model (Singh et al., 2002) is obtained. The plots of the marginal pdf of Θ_1 in (16) are shown in Fig. 5 for $\mu_1 = 0$ and different values of $\kappa_1, \kappa_2, \kappa_3$ and r_1. As can be seen, the distribution can be both unimodal and bimodal. In the following theorem, the bimodality of the marginal pdf of Θ_1 in (16) is discussed.

Theorem 2.6. *The marginal distribution of* Θ_1 *in* (16) *is symmetric around* $\theta_1 = \mu_1$ *and unimodal (with mode at* μ_1*) if and only if* $\frac{A(\kappa_2)}{\kappa_2} \leq \left(\frac{2r_1(1-r_1)^2}{(1-r_1^2)^2} + \kappa_1\right)/\kappa_3^2$ *where* $A(\kappa) = I_1(\kappa)/I_0(\kappa)$. *Also, the marginal distribution of* Θ_1 *in* (16) *is bimodal (with the modes at* $\mu_1 - \theta_1^*$ *and* $\mu_1 + \theta_1^*$*) if and only if* $\frac{A(\kappa_2)}{\kappa_2} > \left(\frac{2r_1(1-r_1)^2}{(1-r_1^2)^2} + \kappa_1\right)/\kappa_3^2$ *and* θ_1^* *is the result of* $\kappa_3^2(1-r_1^2)^2\cos\theta_1^* A(h(\theta_1^*))/h(\theta_1^*) - 2r_1(1+r_1^2-2r_1\cos(\theta_1^* - \mu_1)) - \kappa_1(1-r_1^2)^2 = 0$ *where* $h(\theta)$ *is defined in* (17).

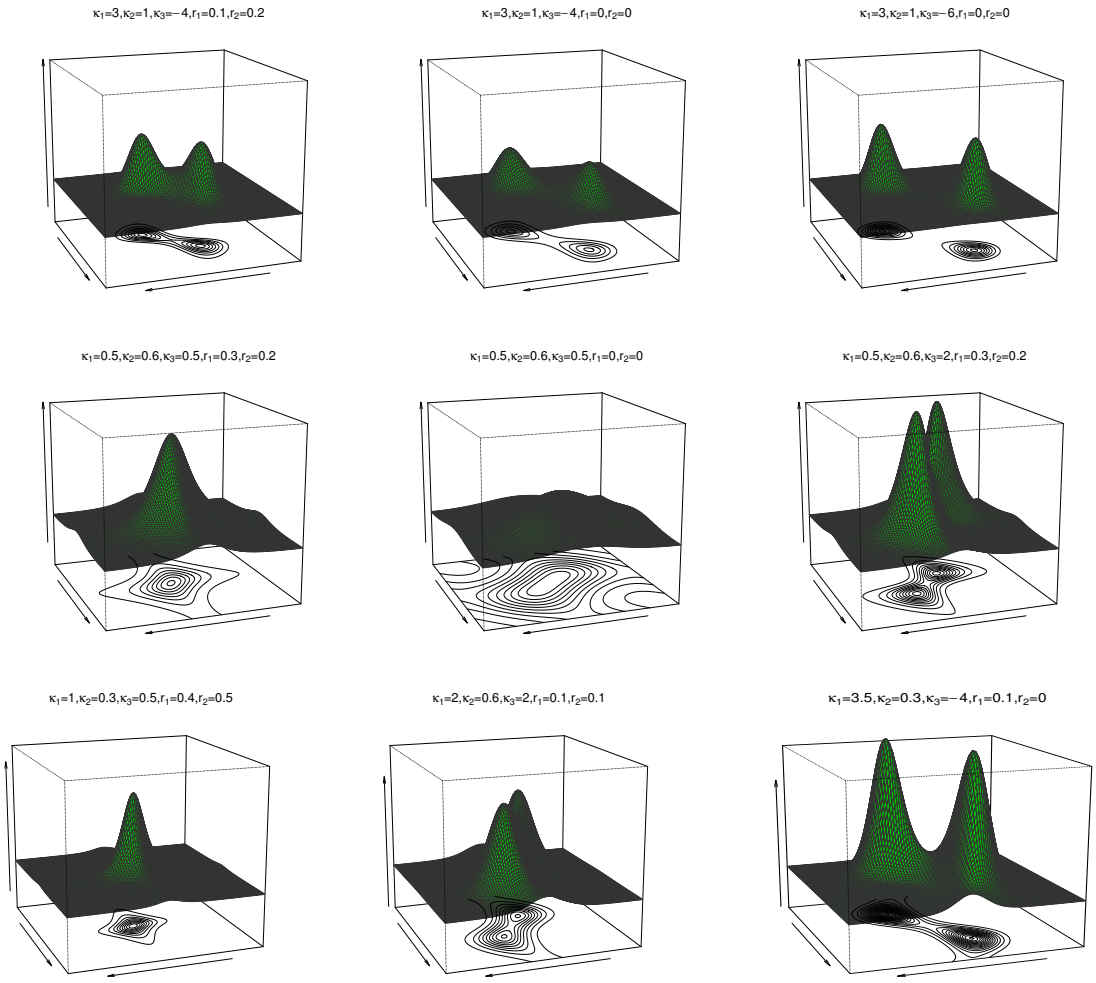

Figure 4: The pdf and contour plots of the transformed Sine model in (14) for $\mu_1 = \mu_2 = 0$ and different values of $\kappa_1, \kappa_2, \kappa_3, r_1$ and r_2.

Proof. Suppose $\mu_1 = 0$ (without loss of generality). According to (16), the result can be obtained that:

$$\begin{aligned}\frac{f'_{\Theta_1}(\theta_1)}{f_{\Theta_1}(\theta_1)} &= \Bigg\{ \frac{-2r_1}{(1+r_1^2-2r_1\cos\theta_1)} - \frac{\kappa_1(1-r_1^2)^2}{(1+r_1^2-2r_1\cos\theta_1)^2} + \frac{\kappa_3^2(1-r_1^2)^2 A(h(\theta_1))}{h(\theta_1)(1+r_1^2-2r_1\cos\theta_1)^4} \\ &\quad \times \left(((1+r_1^2)^2+4r_1^2)\cos\theta_1 - 4r_1(1+r_1^2)\cos^2\theta_1 - 2r_1(1+r_1^2)\sin^2\theta_1\right)\Bigg\}\sin\theta_1 \\ &= g(\theta_1)\sin\theta_1. \end{aligned} \tag{18}$$

In (18), if $\cos\theta_1 \leq 0$, then $g(\theta_1) < 0$ and the sign of (18) depends on the sign of $\sin\theta_1$. So, for $\theta_1 \in (-\pi, -\pi/2]$, $f'_{\Theta_1}(\theta_1) < 0$ and for $\theta_1 \in [\pi/2, \pi]$, $f'_{\Theta_1}(\theta_1) \geq 0$. Thus, $f_{\Theta_1}(\theta_1)$ is increasing in $(-\pi, -\pi/2]$ and decreasing from $\pi/2$ to π. In addition, $f_{\Theta_1}(\theta_1) = f_{\Theta_1}(-\theta_1)$, which means that $f_{\Theta_1}(\theta_1)$ is symmetric around 0; so, $f_{\Theta_1}(\theta_1)$ is unimodal. For $\theta \in [0, \pi/2]$, $h(\theta_1)$ is an increasing function of θ_1, and according to Lemma 1 in Singh et al. (2002), $A(h(\theta_1))/h(\theta_1)$ is a decreasing function of θ_1. It can be concluded that if $-2r(1-r_1)^2 - \kappa_1(1-r_1^2)^2 + \kappa_3^2(1-r_1^2)^2\frac{A(\kappa_2)}{\kappa_2} < 0$, then $f_{\Theta_1}(\theta_1)$ is a decreasing function from 0 to $\pi/2$, and since $f_{\Theta_1}(\theta_1)$ is

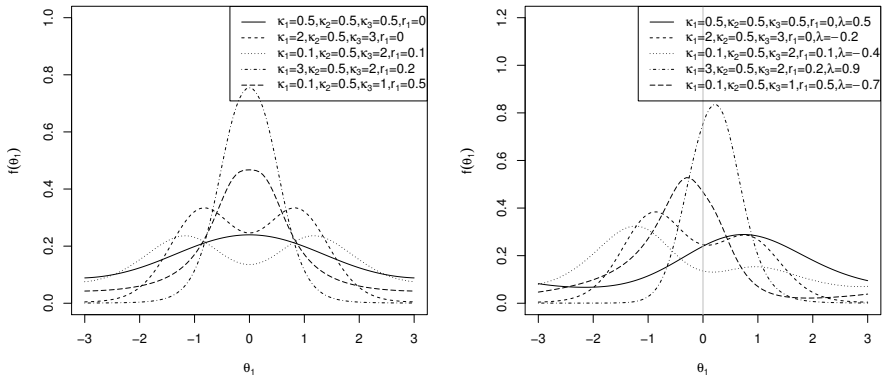

Figure 5: The plots of the marginal pdf of Θ_1 in (16) (left) and the skewed marginal pdf of Θ_1 in (19) (right) for $\mu_1 = 0$ and different values of parameters.

symmetric around 0, it is increasing from $-\pi/2$ to 0. If $-2r(1-r_1)^2 - \kappa_1(1-r_1^2)^2 + \kappa_3^2(1-r_1^2)^2\frac{A(\kappa_2)}{\kappa_2} > 0$, then $f_{\Theta_1}(\theta_1)$ is first increasing and then decreasing in $[0, \pi/2]$ and in $[-\pi/2, 0]$ as well (because of being symmetric around 0), which means that $f_{\Theta_1}(\theta_1)$ is bimodal. □

The sine-skewed (Abe and Pewsey, 2011) version of the marginal pdf of Θ_1 in (16) is:

$$f_{\Theta_1}(\theta_1) = \frac{2\pi C(1-r_1^2)}{1+r_1^2-2r_1\cos(\theta_1-\mu_1)} I_0(h(\theta_1)) \exp\left\{\frac{\kappa_1(1+r_1^2)\cos(\theta_1-\mu_1) - 2\kappa_1 r_1}{1+r_1^2-2r_1\cos(\theta_1-\mu_1)}\right\} \times (1+\lambda\sin(\theta_1-\mu_1)), \tag{19}$$

where C is defined in (3), $h(\theta_1)$ is defined in (17), and $-1 \le \lambda \le 1$. $\lambda > 0$ leads to left-skewed distributions and $\lambda < 0$ provides right-skewed distributions. The plots of the skewed pdf in (19) are shown in Fig. 5 for $\mu_1 = 0$ and different values of $\kappa_1, \kappa_2, \kappa_3, r_1$ and λ.

The conditional pdf $f(\theta_2 \mid \Theta_1 = \theta_1)$ is given by:

$$f(\theta_2 \mid \Theta_1 = \theta_1) = \frac{1-r_2^2}{2\pi I_0(h(\theta_1))} \frac{1}{1+r_2^2-2r_2\cos(\theta_2-\mu_2)} \times \exp\left\{\frac{h(\theta_1)\cos\tau((1+r_2^2)\cos(\theta_2-\mu_2)-2r_2) + h(\theta_1)\sin\tau(1-r_2^2)\sin(\theta_2-\mu_2)}{1+r_2^2-2r_2\cos(\theta_2-\mu_2)}\right\}, \tag{20}$$

where $tan\tau = \frac{\kappa_3}{\kappa_2}\frac{(1-r_1^2)\sin(\theta_1-\mu_1)}{1+r_1^2-2r_1\cos(\theta_1-\mu_1)}$. The conditional distribution is the transformed von Mises distribution (Kato and Jones, 2010). When $r_1 = 0$ in (20), the von Mises distribution with parameter τ and $h(\theta_1)$ is obtained.

3 Sine-Skewed Transformed Sine and Cosine Distributions

On occasion, it is possible to be faced with skewed toroidal data sets, whereas the well-known toroidal distributions are symmetric. Therefore, it would be of interest to extend this methodology to the recent model of Ameijeiras-Alonso and Ley (2019). In this section, the skewed versions of the proposed transformed

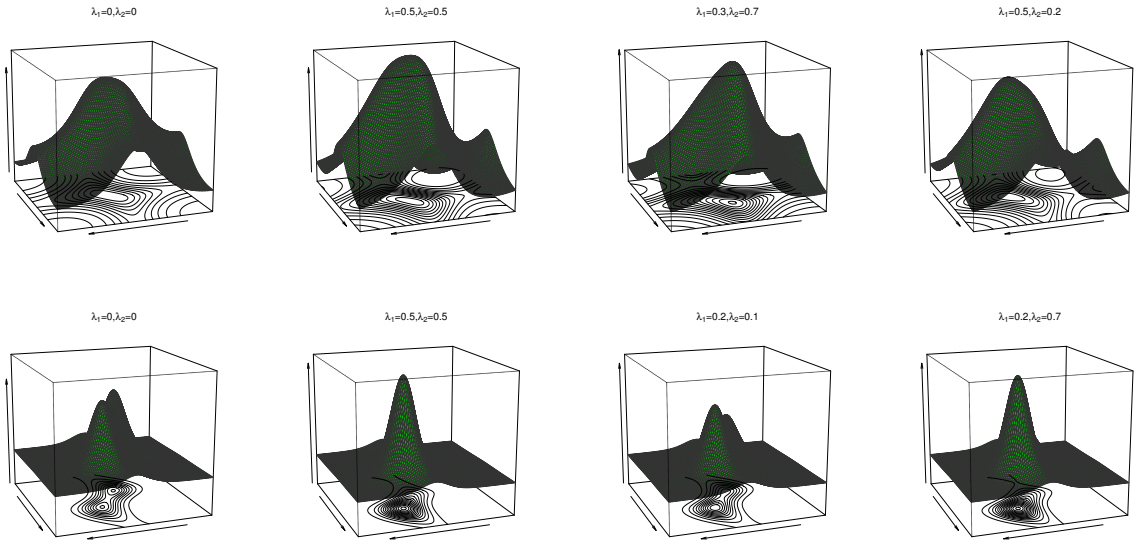

Figure 6: The pdf and contour plots of the sine-skewed transformed Cosine model in (22) (top) and the sine-skewed transformed Sine model in (23) (bottom) for different values of λ_1 and λ_2.

Sine and Cosine models in (14) and (7) are introduced. Ameijeiras-Alonso and Ley (2019) introduced the bivariate sine-skewed distributions as:

$$f_{BSS}(\theta_1,\theta_2) = f(\theta_1-\mu_1,\theta_2-\mu_2)\left(1+\lambda_1\sin(\theta_1-\mu_1)+\lambda_2\sin(\theta_2-\mu_2)\right), \tag{21}$$

where $-1 \leq \lambda_i \leq 1$, $i=1,2$ and $|\lambda_1|+|\lambda_2| \leq 1$. Therefore, by substituting (7) in (21), the *sine-skewed transformed Cosine* ($BSSC$) distribution can be defined as:

$$\begin{aligned} f_{BSSC}(\theta_1,\theta_2) &= \frac{C(1-r_1^2)(1-r_2^2)}{(1+r_1^2-2r_1\cos(\theta_1-\mu_1))(1+r_2^2-2r_2\cos(\theta_2-\mu_2))} \\ &\times \exp\left\{\frac{1}{(1+r_1^2-2r_1\cos(\theta_1-\mu_1))(1+r_2^2-2r_2\cos(\theta_2-\mu_2))}\left(C_0+C_1\cos(\theta_1-\mu_1)\right.\right. \\ &\left.\left.+C_2\cos(\theta_2-\mu_2)+C_3\cos(\theta_1-\mu_1)\cos(\theta_2-\mu_2)+C_4\sin(\theta_1-\mu_1)\sin(\theta_2-\mu_2)\right)\right\} \\ &\times\left(1+\lambda_1\sin(\theta_1-\mu_1)+\lambda_2\sin(\theta_2-\mu_2)\right), \end{aligned} \tag{22}$$

where $\kappa_1,\kappa_2 \geq 0$, $\kappa_3 \in \mathbb{R}$, C is defined in (5) and C_0–C_4 are defined in (8). The pdf and contour plots of the sine-skewed transformed Cosine model for $\kappa_1=0.2$, $\kappa_2=0.3$, $\kappa_3=0.2$, $r_1=0.2$, $r_2=0.1$, $\mu_1=\mu_2=0$ and different values of λ_1 and λ_2 are shown in Fig. 6.

From (14) and (21), the *sine-skewed transformed sine* ($BSSS$) distribution is obtained as:

$$\begin{aligned} f_{BSSS}(\theta_1,\theta_2) &= \frac{C(1-r_1^2)(1-r_2^2)}{(1+r_1^2-2r_1\cos(\theta_1-\mu_1))(1+r_2^2-2r_2\cos(\theta_2-\mu_2))} \\ &\times \exp\left\{\frac{1}{(1+r_1^2-2r_1\cos(\theta_1-\mu_1))(1+r_2^2-2r_2\cos(\theta_2-\mu_2))}\left(C_0+C_1\cos(\theta_1-\mu_1)\right.\right. \\ &\left.\left.+C_2\cos(\theta_2-\mu_2)+C_3\cos(\theta_1-\mu_1)\cos(\theta_2-\mu_2)+C_4\sin(\theta_1-\mu_1)\sin(\theta_2-\mu_2)\right)\right\} \end{aligned} \tag{23}$$

$$\times (1 + \lambda_1 \sin(\theta_1 - \mu_1) + \lambda_2 \sin(\theta_2 - \mu_2)) ,$$

where $\kappa_1, \kappa_2 \geq 0$, $\kappa_3 \in \mathbb{R}$, C is defined in (3) and C_0–C_4 are defined in (15). The pdf and contour plots of the sine-skewed transformed Sine model for $\kappa_1 = 2$, $\kappa_2 = 0.6$, $\kappa_3 = 2$, $r_1 = 0.1$, $r_2 = 0.1$, $\mu_1 = \mu_2 = 0$ and different values of λ_1 and λ_2 are shown in Fig. 6.

4 Maximum Likelihood Estimation

Suppose $\boldsymbol{\zeta} = (\mu_1, \mu_2, \kappa_1, \kappa_2, \kappa_3, r_1, r_2)^T$ is the vector parameter of the transformed Cosine model in (7). The log-likelihood function of the transformed Cosine model can be represented as follows:

$$\begin{aligned} l(\boldsymbol{\zeta}) &= nlogC + nlog(1 - r_1^2) + nlog(1 - r_2^2) - \sum_{i=1}^{n} log(1 + r_1^2 - 2r_1 \cos\theta_{1i}) \\ &- \sum_{i=1}^{n} log(1 + r_2^2 - 2r_2 \cos\theta_{2i}) + \sum_{i=1}^{n} \frac{1}{(1 + r_1^2 - 2r_1 \cos(\theta_{1i} - \mu_1))(1 + r_2^2 - 2r_2 \cos(\theta_{2i} - \mu_2))} \\ &\times (C_0 + C_1 \cos(\theta_{1i} - \mu_1) + C_2 \cos(\theta_{2i} - \mu_2) + C_3 \cos(\theta_{1i} - \mu_1)\cos(\theta_{2i} - \mu_2) \\ &+ C_4 \sin(\theta_{1i} - \mu_1)\sin(\theta_{2i} - \mu_2)) , \end{aligned} \tag{24}$$

where C is defined in (5) and C_0–C_4 are defined in (8). The MLE of parameters, $\hat{\boldsymbol{\zeta}} = (\hat{\mu}_1, \hat{\mu}_2, \hat{\kappa}_1, \hat{\kappa}_2, \hat{\kappa}_3, \hat{r}_1, \hat{r}_2)^T$ can be found by maximizing (24) with respect to $\boldsymbol{\zeta} = (\mu_1, \mu_2, \kappa_1, \kappa_2, \kappa_3, r_1, r_2)^T$.

Suppose $\boldsymbol{\zeta} = (\mu_1, \mu_2, \kappa_1, \kappa_2, \kappa_3, r_1, r_2)^T$ is the vector parameter of the transformed Sine model in (14), then the log-likelihood function of the transformed Sine model can be represented as follows:

$$\begin{aligned} l(\boldsymbol{\zeta}) &= nlogC + nlog(1 - r_1^2) + nlog(1 - r_2^2) - \sum_{i=1}^{n} log(1 + r_1^2 - 2r_1 \cos\theta_{1i}) \\ &- \sum_{i=1}^{n} log(1 + r_2^2 - 2r_2 \cos\theta_{2i}) + \sum_{i=1}^{n} \frac{1}{(1 + r_1^2 - 2r_1 \cos(\theta_{1i} - \mu_1))(1 + r_2^2 - 2r_2 \cos(\theta_{2i} - \mu_2))} \\ &\times (C_0 + C_1 \cos(\theta_{1i} - \mu_1) + C_2 \cos(\theta_{2i} - \mu_2) + C_3 \cos(\theta_{1i} - \mu_1)\cos(\theta_{2i} - \mu_2) \\ &+ C_4 \sin(\theta_{1i} - \mu_1)\sin(\theta_{2i} - \mu_2)) , \end{aligned} \tag{25}$$

where C is defined in (5) and C_0–C_4 are defined in (15). Maximization of (25) with respect to $\boldsymbol{\zeta} = (\mu_1, \mu_2, \kappa_1, \kappa_2, \kappa_3, r_1, r_2)^T$ results in the MLE of parameters, $\hat{\boldsymbol{\zeta}} = (\hat{\mu}_1, \hat{\mu}_2, \hat{\kappa}_1, \hat{\kappa}_2, \hat{\kappa}_3, \hat{r}_1, \hat{r}_2)^T$.

5 Application: Protein Structure

To demonstrate the performance of the proposed models in the previous sections for modeling of the dihedral angles and planar and torsion angles in the structure of proteins, three data sets are considered. SCOP.1 contains 10188 planar and torsion angles (θ, τ) (see Fig. 1(A)) for about 63 protein domains that were randomly selected from three remote protein classes in the Structural Classification of Proteins (SCOP), which is available at http://scop.mrc-lmb.cam.ac.uk/scop/. SCOP.3 includes 4607 planar and torsion angles (θ, τ) for about 40 protein chains, and the TCBIG.VAL.right set consists of 2673 dihedral angles (ϕ, ψ) (see Fig. 5(B)) (Najibi et al., 2017). The Ramachandran plots (Ramachandran and Sasisekharan, 1968) for the data sets are shown in Fig. 7. The transformed Sine and Cosine models in (14) and (7) along with their competitors, namely the Sine model in (2) (Singh et al., 2002), the Cosine model in (4) (Mardia et al., 2007) and the bivariate wrapped Cauchy model (Kato and Pewsey, 2015), are fitted to SCOP.1 and SCOP.3 data

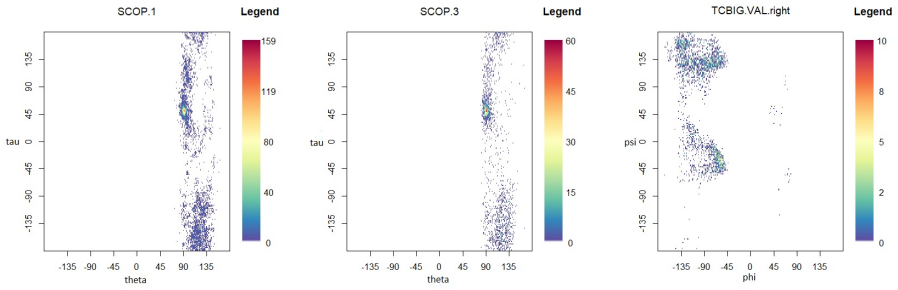

Figure 7: The Ramachandran plots for the data sets.

sets. The results, including the MLE of parameters, log-likelihood, Akaike information criterion (AIC) and Bayesian information criterion (BIC), are shown in Tables 1 and 2. As can be seen in Tables 1 and 2, the transformed Sine model in (14) provides the best fit on the data. The scatter plots of the data and the contour plots of fitted distributions are shown in Figs 8 and 9.

Table 1: Maximum likelihood estimates and corresponding standard errors and log-likelihood, AIC and BIC for SCOP.1 ($n = 10188$)

Model	$\hat{\kappa_1}$	$\hat{\kappa_2}$	$\hat{\kappa_3}$	$\hat{r_1}$	$\hat{r_2}$	$\hat{\mu_1}$	$\hat{\mu_2}$	Log-likelihood	AIC	BIC
Sine	25.2085	0.3679	7.3700	–	–	1.8976	2.4624	−15890.80	31790.16	31827.74
(Singh et al., 2002)										
Cosine	11.6274	6.7e-17	0.6507	–	–	1.8807	−0.8652	−19919.04	39848.07	39884.22
(Mardia et al., 2007)										
Bivariate Wrapped Cauchy	0.6098	–	–	0.8110	0.1181	1.7508	1.9390	−18319.90	36649.81	36685.94
(Kato and Pewsey, 2015)										
Transformed Sine	2.1585	0.3489	3.1712	0.6036	0.0131	1.8573	2.4321	−15558.98	**31131.97**	**31182.56**
Transformed Cosine	4.5122	1.9e-16	2.7905	0.2632	0.4164	1.8806	−0.6888	−16920.43	33854.86	33905.46

Table 2: Maximum likelihood estimates and corresponding standard errors and log-likelihood, AIC and BIC for SCOP.3 ($n = 4607$)

Model	$\hat{\kappa_1}$	$\hat{\kappa_2}$	$\hat{\kappa_3}$	$\hat{r_1}$	$\hat{r_2}$	$\hat{\mu_1}$	$\hat{\mu_2}$	Log-likelihood	AIC	BIC
Sine	27.0312	0.3243	8.0789	–	–	1.8810	2.4618	−6970.09	13950.18	13982.36
(Singh et al., 2002)										
Cosine	11.5883	3.8e-16	0.6404	–	–	1.8537	-0.9851	−9028.72	18067.45	18099.62
(Mardia et al., 2007)										
Bivariate Wrapped Cauchy	0.5968	–	–	0.8122	0.1265	1.7322	1.8487	−8265.40	16540.80	16572.98
(Kato and Pewsey, 2015)										
Transformed Sine	3.8755	0.3414	3.6786	0.4950	1.3e-09	1.8589	2.4490	−6905.08	**13824.17**	**13869.22**
Transformed Cosine	4.1351	2.4e-16	2.8283	0.2884	0.4183	1.8604	-0.6560	−7567.28	15148.56	15193.61

For the last data set TCBIG.VAL.right, in addition to the transformed Sine and Cosine distributions in (14) and (7), the Sine model in (2), the Cosine models in (4) and the bivariate wrapped Cauchy distribution (Kato and Pewsey, 2015), the sine-skewed version of the transformed Sine and Cosine distributions in (23) and (22) and also the sine-skewed version of the other models mentioned above (Ameijeiras-Alonso and Ley, 2019) are considered. The results are summarized in Table 3. As can be seen in Table 3, the transformed Cosine model and sine-skewed transformed Cosine model provide the best fit on the data. Based on the

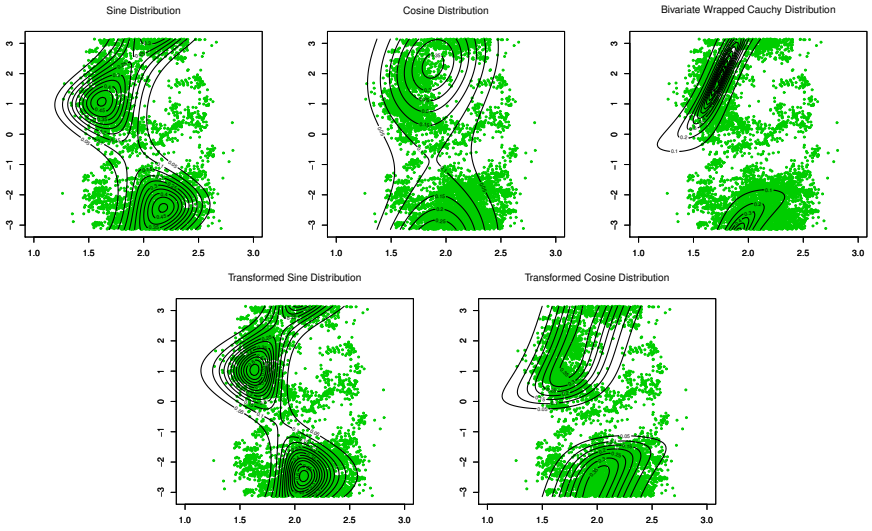

Figure 8: The fitted pdf plots and contour plots for SCOP.1 ($n = 10188$).

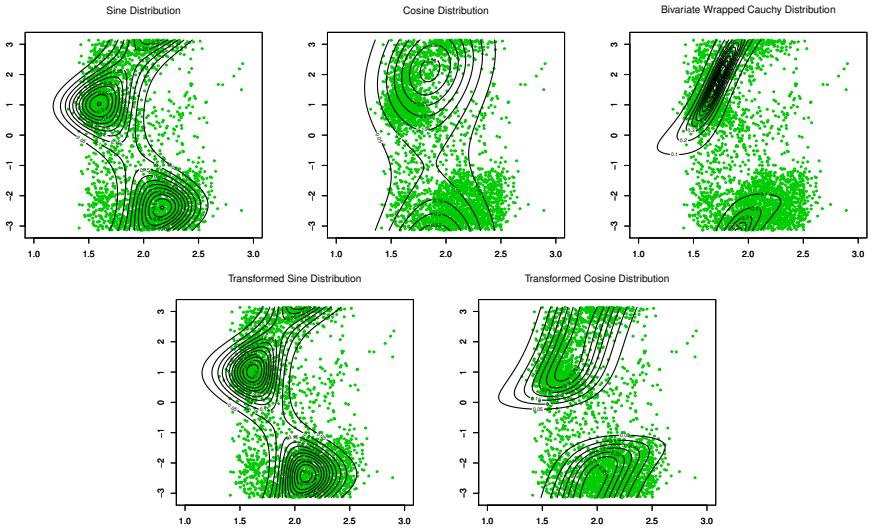

Figure 9: The fitted pdf plots and contour plots for SCOP.3 ($n = 4607$).

symmetry test of Ameijeiras-Alonso and Ley (2019) and the values of log-likelihood in Table 3, there is no evidence to reject that the underlying distribution for the TCBIG.VAL.right data set is symmetric except for the Sine distribution. The transformed Sine model in (14) is the third-best model. The scatter plots of the data and the contour plots of the fitted distributions are shown in Fig. 10.

Table 3: Maximum likelihood estimates and corresponding standard errors and log-likelihood, AIC and BIC for TCBIG.VAL.right ($n = 2673$).

Model	$\hat{\kappa_1}$	$\hat{\kappa_2}$	$\hat{\kappa_3}$	$\hat{r_1}$	$\hat{r_2}$	$\hat{\mu_1}$	$\hat{\mu_2}$	$\hat{\lambda_1}$	$\hat{\lambda_2}$	Log-likelihood	AIC	BIC
Sine	4.7016	0.5051	−1.6266	–	–	−1.5777	1.2167	–	–	−6615.00	13240.01	13269.45
(Singh et al., 2002)												
Sine-Skewed Sine	4.0811	0.3866	0.3672	–	–	−1.6162	2.7297	−0.0016	−0.9923	−6577.06	13168.12	13209.36
Cosine	4.0476	0.6067	1.4e-16	–	–	−1.6368	1.8687	–	–	−6824.88	13659.76	13689.21
(Mardia et al., 2007)												
Sine-Skewed Cosine	4.0435	0.6182	2.2e-10	–	–	−1.6372	1.8517	−0.1589	0.0738	−6825.01	13664.02	13705.26
Bivariate Wrapped Cauchy	−0.0509	–	–	0.6726	0.5361	−1.5869	2.2763	–	–	−7118.71	14242.42	14276.87
(Kato and Pewsey, 2015)												
Sine-Skewed Bivariate Wrapped Cauchy	−0.0512	–	–	0.6751	0.5409	−1.7675	2.2746	0.4971	−0.4052	−7118.67	14253.35	14292.58
Transformed Sine	3.7691	0.4985	−1.5337	0.0775	9.8e-07	−1.5741	1.1944	–	–	−6603.41	13220.82	13262.06
Sine-Skewed Transformed Sine	3.7693	0.4979	−1.5348	0.0778	2.0e-08	−1.5738	1.1943	−0.3382	0.4679	−6603.40	13224.81	13277.82
Transformed Cosine	3.9891	3.1e-17	1.7911	4.1e-16	0.5046	−1.5651	0.9878	–	–	−6529.09	**13072.18**	**13113.42**
Sine-Skewed Transformed Cosine	3.9892	4.2e-11	1.7914	1.3e-07	0.5046	−1.5652	0.9878	−0.2548	0.0110	−6529.09	13076.18	13129.20

6 Simulation Study

In this section, for simulating a sample from the newly proposed transformed Sine and transformed Cosine distributions in (14) and (7), four packages in R, including MCMCpack (Martin et al., 2020), gibbs.met (Li, 2015), LearnBayes (Albert, 2018) and MHadaptive (Chivers and Chivers, 2015), are used and the results are compared. First, a sample of size $n = 1000$ is generated with each package from the transformed Sine model in (14) with parameters $\kappa_1 = 2.1585$, $\kappa_2 = 0.3489$, $\kappa_3 = 3.1712$, $r_1 = 0.6036$, $r_2 = 0.0131$, $\mu_1 = 1.8573$ and $\mu_2 = 2.4321$, the best-fitted model for the SCOP.1 data set in the previous section. The results, including the simulated sample with the contour plot of the distribution, the trace plot and the compare-partial plot (Fernández-i-Marín, 2016) which compares the last 10 per cent of values in the chain with the whole chain, are shown in Fig. 11. The run-time of each method is shown in Table 4 and Fig. 12 (Mersmann et al., 2019). The MLE of the parameters, bias and mean squared error (MSE) of the estimates are calculated for each method, using the Monte Carlo method with 500 replications and $n = 1000$. The results are summarized in Table 5. As can be seen, the gibbs_met method provides the best results, despite the low speed.

Similarly, for the transformed Cosine model in (7) with parameters $\kappa_1 = 3.9891$, $\kappa_2 = 3.1e-17$,$\kappa_3 = 1.7911$,$r_1 = 4.1e-16$, $r_2 = 0.5046$, $\mu_1 = -1.5651$ and $\mu_2 = 0.9878$ (the best model for the TCBIG.VAL.right data set in the previous section), the mentioned R packages are applied to generate a sample size of $n = 1000$. The results, including the simulated sample with the contour plot of the distribution, the trace plot and the compare-partial plot (Fernández-i-Marın, 2016) are shown in Fig. 13. The run-time of each method is shown in Table 4 and Fig. 12 (Mersmann et al., 2019). The MLE of the parameters, bias and MSE of the estimates are calculated for each method, using the Monte Carlo method with 500 replications and $n = 1000$. The results are summarized in Table 5. As can be seen, the MCMCmetrop1R is a high-speed method that provides the best results.

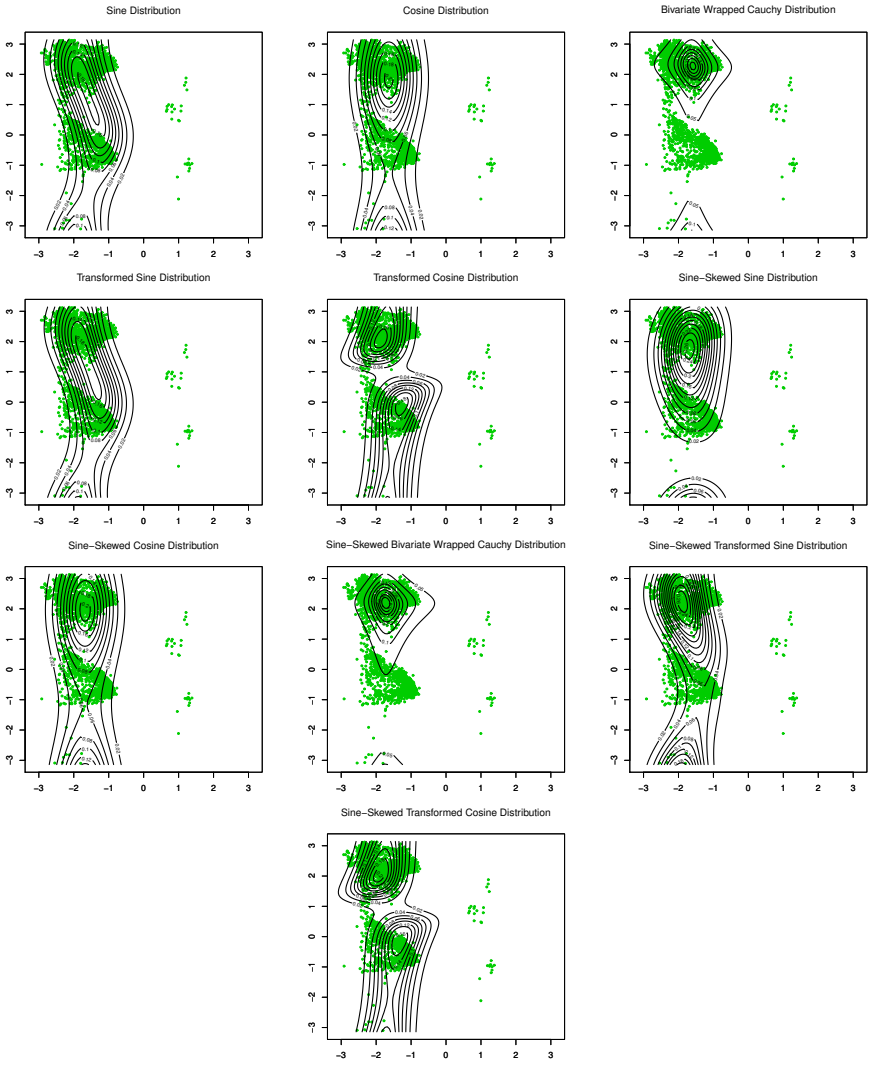

Figure 10: The fitted pdf plots and contour plots for TCBIG.VAL.right ($n = 2673$).

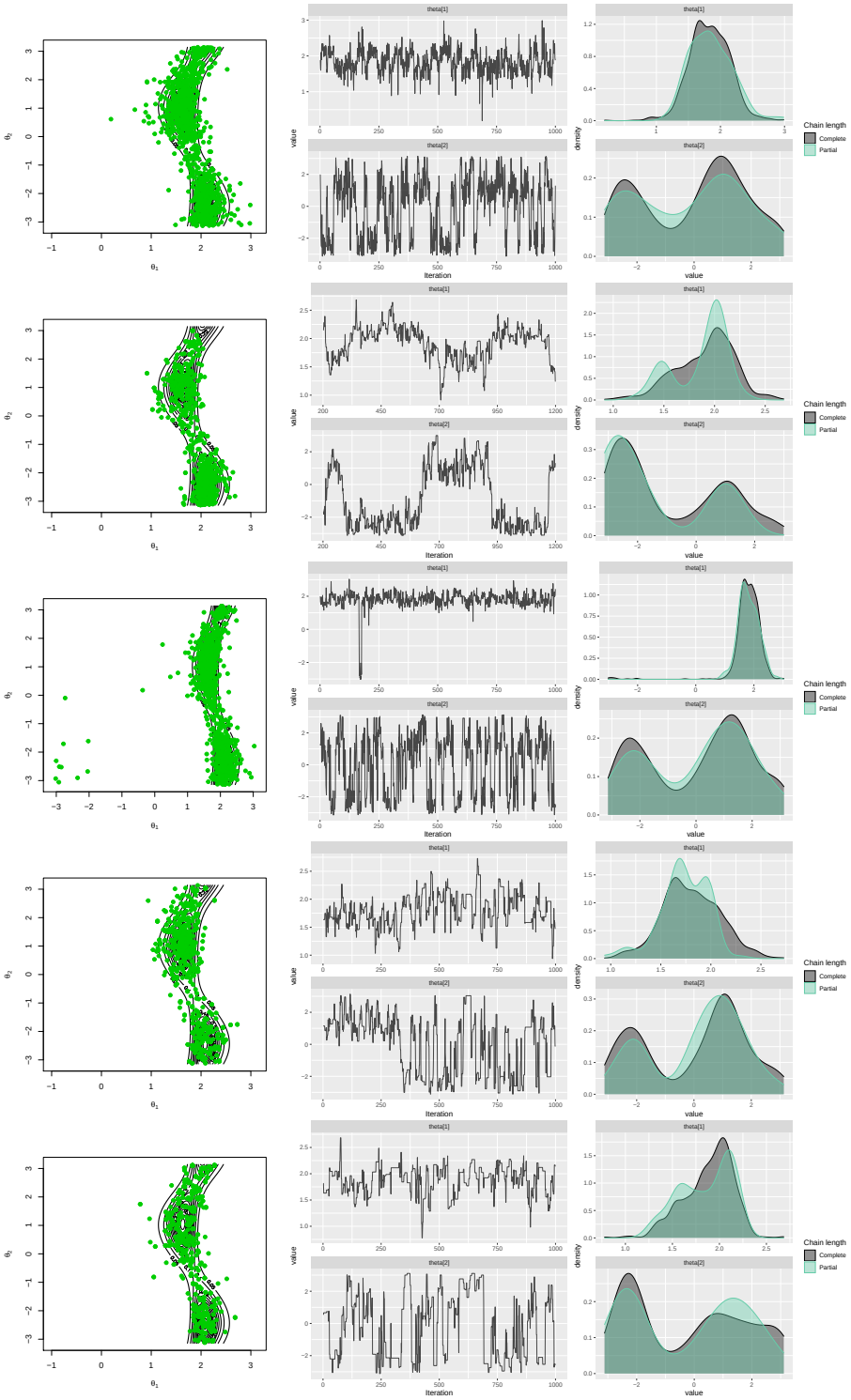

Figure 11: The simulated data with the "gibbs_met" in the "gibbs.met" package (first row),the "MCMCmetrop1R" in the "MCMCpack" package (second row), the "met_gaussian" in the "gibbs.met" package (third row), the "Metro_Hastings" in the "MHadaptive" package (fourth row) and the "rwmetrop" in the "LearnBayes" package (fifth row).

Table 4: The execution time for generating a sample size of $n = 100$ for each method (Unit: milliseconds).

method	Distribution	min	Q_1	mean	median	Q_3	max
MCMCmetrop1R	Transformed Sine	82.44273	89.96106	108.4854	92.40256	97.43003	229.1553
	Transformed Cosine	418.6131	445.1546	493.5413	454.7127	461.7519	953.1217
rwmetrop	Transformed Sine	127.14246	131.06110	152.2298	134.43100	140.29252	305.8380
	Transformed Cosine	637.5074	666.6106	715.3140	682.0742	693.0377	1544.8174
met_gaussian	Transformed Sine	606.80692	625.16437	705.8385	640.60429	650.72400	2088.1971
	Transformed Cosine	3171.6330	3308.5453	3602.8474	3412.6115	3833.1665	5018.7944
Metro_Hastings	Transformed Sine	202.40434	211.77995	240.7471	215.82223	221.57837	522.7105
	Transformed Cosine	898.7989	938.0609	1013.3572	964.7982	987.3257	2370.7001
gibbs_met	Transformed Sine	1507.63116	1538.99756	1681.0145	1586.65002	1670.04196	3055.7828
	Transformed Cosine	7780.3871	200.3594	8920.0251	8936.5964	9598.0682	10603.6552

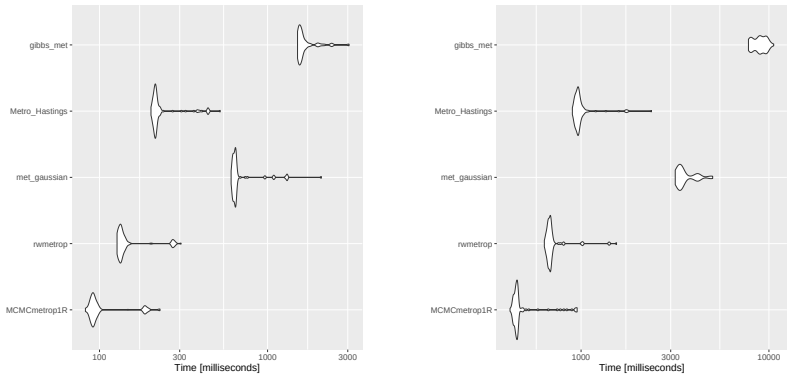

Figure 12: The execution time for generating a sample size of $n = 100$ from transformed Sine model (left) and transformed Cosine model (right) for each method.

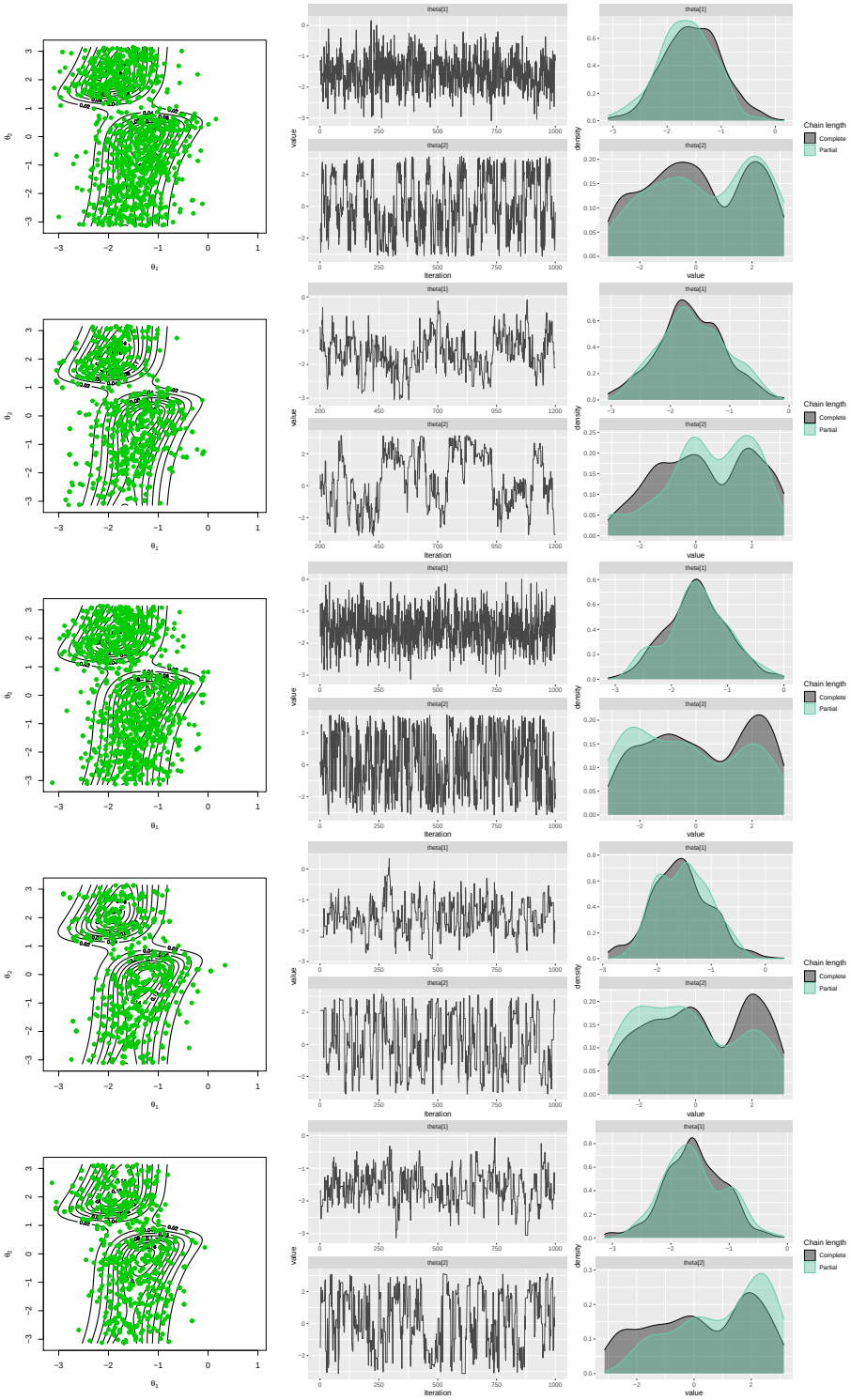

Figure 13: The simulated data with the "gibbs_met" in the "gibbs.met" package (first row),"MCMCmetrop1R" in the "MCMCpack" package (second row), "met_gaussian" in the "gibbs.met" package (third row), "Metro_Hastings" in the "MHadaptive" package (fourth row) and "rwmetrop" in the "LearnBayes" package (fifth row).

Table 5: The Maximum likelihood estimates of parameters, bias and MSE for each method.

Method	Distribution		κ_1	κ_2	κ_3	r_1	r_2	μ_1	μ_2
		MLE	0.0205	−0.1981	−0.7061	0.0016	0.0323	−0.0007	0.0144
	Transformed Sine	Bias	2.1791	0.1507	2.4650	0.6052	0.0454	1.8565	2.4465
		MSE	0.1152	0.0690	0.8447	0.0012	0.0018	0.0002	0.0140
MCMCmetrop1R									
		MLE	4.0815	4.4e-13	1.8596	1.8e-11	0.5082	−1.5586	0.9805
	Transformed Cosine	Bias	0.0924	4.4e-13	0.0685	1.8e-11	0.0036	0.0064	−0.0072
		MSE	0.0803	8.6e-25	0.0281	1.3e-21	0.0009	0.0004	0.0017
		MLE	0.2965	0.0398	−0.4735	−0.0062	0.0031	0.0087	−0.0026
	Transformed Sine	Bias	2.4550	0.3887	2.6976	0.5973	0.0162	1.8660	2.4294
		MSE	0.2393	0.0289	0.5300	0.0013	0.0005	0.0007	0.0032
rwmetrop									
		MLE	4.0611	3.8e-10	1.8050	0.0157	0.4929	−1.5024	1.0332
	Transformed Cosine	Bias	0.0720	3.8e-10	0.0139	0.0157	−0.0116	0.0626	0.0454
		MSE	0.2982	9.7e-19	0.0323	0.0009	0.0019	0.0066	0.0005
		MLE	0.1136	−0.0287	−1.3236	−0.0083	0.0133	−0.0037	−0.0050
	Transformed Sine	Bias	2.2947	0.3201	1.8475	0.5952	0.0264	1.8534	2.4271
		MSE	0.0708	0.0359	1.1478	0.0005	0.0010	5.4e-05	0.0012
met_gaussian									
		MLE	4.0396	1.1e-10	1.6982	0.0099	0.4834	−1.5613	0.9946
	Transformed Cosine	Bias	0.0505	1.1e-10	−0.0928	0.0099	−0.0211	0.0037	0.0068
		MSE	0.1145	8.3e-20	0.0241	0.0006	0.0007	0.0002	0.0007
		MLE	2.8019	0.3190	2.7665	0.5736	0.0272	1.8506	2.3672
	Transformed Sine	Bias	0.6434	−0.0298	−0.3746	−0.0299	0.0141	−0.0066	−0.0648
		MSE	0.6193	0.0640	0.6933	0.0018	0.0013	0.0006	0.0112
Metro_Hastings									
		MLE	3.8324	6.1e-10	1.8190	0.0252	0.5168	−1.5521	0.9803
	Transformed Cosine	Bias	−0.1566	6.1e-10	0.0279	0.0252	0.0122	0.0129	−0.0074
		MSE	0.3103	2.8e-18	0.0381	0.0019	0.0012	0.0019	0.0056
		MLE	2.1901	0.3555	3.1760	0.6016	0.0156	1.8573	2.4342
	Transformed Sine	Bias	0.0315	0.0066	0.00485	−0.0020	0.0024	6.1e-05	0.0021
		MSE	0.0963	0.0221	0.4647	0.0008	0.0003	1.7e-05	0.0018
gibbs_met									
		MLE	3.8321	7.5e-11	1.7131	0.0219	0.4751	−1.5661	0.9705
	Transformed Cosine	Bias	−0.1570	7.5e-11	−0.0779	0.0219	−0.0294	0.0009	−0.0172
		MSE	0.5448	4.4e-20	0.0186	0.0022	0.0012	0.0001	0.0008

Acknowledgement

This work was based upon research supported in part by the National Research Foundation (NRF) of South Africa, SARChI Research Chair UID: 71199; Ref.: IFR170227223754 grant No. 109214; Ref.: SRUG190308422768 grant No. 120839, and DSI-NRF Centre of Excellence in Mathematical and Statistical Sciences (CoE-MaSS), South Africa. The opinions expressed and conclusions arrived at are those of the authors and are not necessarily to be attributed to the CoE-MaSS or the NRF.

References

ABE, T. & PEWSEY, A. (2011). Sine-skewed circular distributions. *Statistical Papers*, **52**(3), 683-707.

ALBERT, J. (2018). LearnBayes: Functions for Learning Bayesian Inference, R package version 2.15.1.

AMEIJEIRAS-ALONSO, J. & LEY, C. (2019). Sine-skewed toroidal distributions and their application in protein bioinformatics. *arXiv preprint arXiv:1910.13293*.

CHIVERS, C. & CHIVERS, M. C. (2015). MHadaptive: General Markov Chain Monte Carlo for Bayesian Inference using adaptive Metropolis-Hastings sampling, R package version 1.1-8.

DI MARZIO, M., PANZERA, A. & TAYLOR, C. C. (2011). Kernel density estimation on the torus. *Journal of Statistical Planning and Inference*, **141**(6), 2156-2173.

DOWNS, T. D. & MARDIA, K. V. (2002). Circular regression. *Biometrika*, **89**, 683–697.

FERNANDEZ-I-MARIN, X. (2016). ggmcmc: Analysis of MCMC samples and Bayesian inference. *Journal of Statistical Software*, **70**(9), 1-20.

HASTINGS, W. K. (1970). Monte Carlo sampling methods using Markov chains and their applications. *Biometrika*, **57**(1), 97-109.

HOLLEY, L. H. & KARPLUS, M. (1989). Protein secondary structure prediction with a neural network. *Proceedings of the National Academy of Sciences*, **86**(1), 152-156.

HUANG, K. Y., AMODEO, G. A., TONG, L. & MCDeRMOTT, A. (2011). The structure of human ubiquitin in 2-methyl-2,4-pentanediol: A new conformational switch. *Protein Science*, **20**, 630-639.

IRBACK, A. & MOHANTY, S. (2006). PROFASI: a Monte Carlo simulation package for protein folding and aggregation. *Journal of Computational Chemistry*, **27**(13), 1548-1555.

JONES, D. T. (1997). Successful ab initio prediction of the tertiary structure of NK-lysin using multiple sequences and recognized supersecondary structural motifs. *Proteins: Structure, Function, and Bioinformatics*, **29**(S1), 185-191.

JONES, T. A. & THIRUP, S. (1986). Using known substructures in protein model building and crystallography. *The EMBO Journal*, **5**(4), 819-822.

JONES, M. C. (2004). The Möbius distribution on the disc. *Annals of the Institute of Statistical Mathematics*, **56**(4), 733-742.

KATO, S. (2009). A distribution for a pair of unit vectors generated by Brownian motion. *Bernoulli*, **15**, 898–921.

KATO, S. & JONES, M. C. (2010). A family of distributions on the circle with links to, and applications arising from, Möbius transformation. *Journal of the American Statistical Association*, **105**(489), 249-262.

KATO, S. & MCCULLAGH, P. (2015). Möbius transformation and a Cauchy family on the sphere. *arXiv preprint arXiv:1510.07679*.

KATO, S. and PEWSEY, A. (2015). A Möbius transformation-induced distribution on the torus. *Biometrika*, **102**, 359–370.

KATO, S., SHIMIZU, K. & SEIEH, G. S. (2008). A circular–circular regression model. *Statistica Sinica*, **18**, 633-645.

LEY, C. & VERDEBOUT, T. (2017). *Modern Directional Statistics*. Chapman and Hall/CRC Press, Boca Raton, Florida.

LEY, C. & VERDEBOUT, T. (2018). *Applied Directional Statistics: Modern Methods and Case Studies*. Chapman and Hall/CRC Press, Boca Raton, Florida.

LI, L. (2015). gibbs.met: Naive Gibbs Sampling with Metropolis Steps, R package version 1.1-3.

LIU, D., PEDDADA, S. D., LI, L. & WEINBERG, C. R. (2006). Phase analysis of circadian-related genes in two tissues.*BMC Bioinformatics*, **7**(1):87.

MARDIA, K. V. (1975). Statistics of directional data. *Journal of the Royal Statistical Society: Series B (Methodological)*, **37**(3), 349-371.

MARDIA, K. V., TAYLOR, C. C. & SUBRAMANIAM, G. K. (2007). Protein bioinformatics and mixtures of bivariate von Mises distributions for angular data. *Biometrics*, **63**(2), 505-512.

MARTIN, A. D., QUINN, K. M., PARK, J. H. & PARK, M. J. H. (2020). MCMCpack: Markov Chain Monte Carlo (MCMC) Package, R package version 1.4-8.

MCCULLAGH, P. (1996). Möbius transformation and Cauchy parameter estimation. *The Annals of Statistics*, **24**(2), 787-808.

MERSMANN, O. (2019). microbenchmark: Accurate Timing Functions. R package version, 1.4-7.

METROPOLIS, N., ROSENBLUTH, A. W., ROSENBLUTH, M. N., TELLER, A. H. & TELLER, E. (1953). Equation of state calculations by fast computing machines. *The Journal of Chemical Physics*, **21**(6), 1087-1092.

MINH, D. L. & FARNUM, N. R. (2003). Using bilinear transformations to induce probability distributions. *Communications in Statistics-Theory and Methods*, **32**(1), 1-9.

NAJIBI, S. M., MAADOOLIAT, M., ZHOU, L., HUANG, J. Z. & GAO, X. (2017). Protein structure classification and loop modeling using multiple Ramachandran distributions. *Computational and Structural Biotechnology Journal*, **15**, 243-254.

OLSSON, S., BOOMSMA, W., FRELLSEN, J., BOTTARO, S., HARDER, T., FERKINGHOFF-BORG, J. & HAMELRYCK, T. (2011). Generative probabilistic models extend the scope of inferential structure determination. *Journal of Magnetic Resonance*, **213**(1), 182-186.

RAMACHANDRAN, G. T. & SASISEKHARAN, V. (1968). Conformation of polypeptides and proteins. *Advances in Protein Chemistry*, **23**, 283-437.

RIVEST, L. P. (1988). A distribution for dependent unit vectors. *Communications in Statistics*, **A17**, 461-483.

SHIEH, G. S., ZHENG, R. A. JOHNSON, Y. F. CHANG, K. SHIMIZU, C. C. WANG, & S. L. TANG (2011). Modeling and comparing the organization of circular genomes. *Bioinformatics*, **27**, 912–918.

SHIEH, G.S. & JOHNSON, R.A. (2005). Inferences based on a bivariate distribution with von Mises marginals, *Annals of the Institute of Statistical Mathematics*, **57**, 789–802.

SIMONS, K. T., KOOPERBERG, C., HUANG, E. & BAKER, D. (1997). Assembly of protein tertiary structures from fragments with similar local sequences using simulated annealing and Bayesian scoring functions. *Journal of Molecular Biology*, **268**(1), 209-225.

SINGH, H., HNIZDO, V. & DEMCHUK, E. (2002). Probabilistic model for two dependent circular variables. *Biometrika*, **89**, 719-723.

WANG, M. Z. & SHIMIZU, K. (2012). On applying Möbius transformation to cardioid random variables. *Statistical Methodology*, **9**(6), 604-614.

WANG, S., PENG, J., MA, J. & XU, J. (2016). Protein secondary structure prediction using deep convolutional neural fields. *Scientific Reports*, **6**, 1-11.

ZHANG, Y. (2008). Progress and challenges in protein structure prediction. *Current Opinion in Structural Biology*, **18**(3), 342-348.